Transient Liquid-Phase Sintering of Copper-Nickel Powders: In Situ Neutron Diffraction

Turriff, Dennis M.; Corbin, Stephen F.; Cranswick, Lachlan M.D.; Watson, Michael J.

Publisher's version / Version de l'éditeur:

International Journal of Powder Metallurgy, 44, 6, pp. 49-59, 2008

The initial melting behavior and solidification kinetics during transient liquid-phase sintering (TLPS) of elemental copper–nickel powder mixtures have been investigated via in situ neutron diffraction (ND). By conducting ND experiments at various isothermal sintering temperatures and durations above the copper melting point, partial liquation of the powder mixtures was induced. By tracking the post-melt evolution of the (200) diffraction peak profiles during prolonged sintering cycles, insight has been obtained regarding interdiffusion of copper and nickel within the unmelted nickel powder, which is responsible for the diffusional, or isothermal, solidification of the surrounding liquid phase. It is concluded that the transient liquid is removed primarily by the rapid growth of a copper-rich solid solution having a composition given by the phase diagram solidus.

TRANSIENT LIQUID-PHASE SINTERING OF COPPER–NICKEL POWDERS: IN SITU NEUTRON DIFFRACTION

Dennis M. Turriff,* Stephen F. Corbin, Lachlan M.D. Cranswick,*** and Michael J. Watson******

INTRODUCTION

Transient liquid-phase sintering (TLPS) is a unique powder metallurgy (PM) processing technique typically used to form near-net-shape parts[1] and more recently, as in this study, as a means of developing liquid-rich low-temperature solders[2,3] and brazing filler materials[4] that exhibit variable melting point (VMP) characteristics. In TLPS, starting mixtures normally consist of a low-melting-point additive powder and a higher-melting-point base-metal powder. The transient liquid phase that forms during heat-up past the additive's melting point aids in rapid densification of the mixture.[1,5–8] This liquid alloys with the base-metal powder during sintering and can lead to complete isothermal, or diffusional, solidification and a shift in melting point for the bulk powder mixture.[4]

In order to achieve the maximum melting-point shift for VMP brazing applications the isothermally solidified phase should have a completely homogenized composition. The consequence of diffusional solidification and incomplete homogenization was previously studied[4] via differential scanning calorimetry (DSC). DSC results for nickel and copper powder mixtures (65 w/o Cu) showed quantitatively that a hold time of 150 min at 1,140°C enabled complete isothermal solidification of the copper-rich liquid during TLPS. Upon reheating, the TLP-sintered specimens exhibited a measurable melting-point increase, and an enhanced melting range due to incomplete homogenization of the isothermally solidified microstructure. Metallographic characterization of the post-sintered DSC specimens revealed that significant compositional gradients remained between the nickel-rich particle cores and the surrounding copper-rich solid-solution regions, even after holding for 150 min at 1,140°C.[4]

**Instructor/Research Associate, **Professor and Associate Chair of Research, Materials Processing and Engineering Group, Department of Mechanical & Mechatronics Engineering, University of Waterloo, 200 University Avenue W, Bldg. E2-4404, Waterloo, Ontario, Canada, N2L 3G1; E-mail: dmturrif@uwaterloo.ca, ***Research Scientist, ****Research Scientist, Retired, Canadian Neutron Beam Centre, National Research Council Canada, Bldg. 459, Chalk River Laboratories, Chalk River Ontario, Canada, K0J 1J0*

From this discussion, it is clear that interdiffusion between the copper and nickel phases during the isothermal solidification and homogenization stages of TLPS is important in determining the rate of liquid removal at 1,140°C, as well as the extent of melting-point shift. Therefore, the primary objective of this investigation was to develop an experimental method using neutron diffraction (ND) to measure in situ the extent of interdiffusion taking place during TLPS of copper–nickel powders. Rudman and Fischer[9] and Delhez et al.[10] have shown that X-ray diffraction techniques (XRD) can be used to investigate the increasing degree of interdiffusion of copper–nickel during solid-state sintering. This was done by tracking the evolution of the (220) diffraction profiles for copper and nickel after isothermal sintering of copper and nickel powder mixtures below 1,085°C. The gradual formation of alloyed regions within the compacts due to sintering and interdiffusion gave rise to XRD peak broadening and the generation of a wide diffraction signal at all intermediate 2θ angles, since nickel and copper constitute an isomorphous alloy system.

It should be noted that the studies cited focused on solid-state sintering and XRD measurements were done after the sintering treatment (i.e., ex situ). The authors are not aware of any in situ studies on sintering of powder mixtures in the presence of a transient liquid, which inherently complicates the process. The large penetration depth and large representative-sample volumes (grams) offered by monochromatic neutron beams makes them an ideal probe for such investigations.

MATERIALS AND METHODS

Table I lists the copper and nickel powders used and their relevant characteristics. The copper powder represents the low-melting-point additive phase (T_m = 1,085°C) and source of liquid during sintering, whereas the nickel powder represents the high-melting-point base-metal phase (T_m = 1,455°C). Specimens were prepared by mixing the loose elemental powders such that the bulk mixture composition, (C_O) was 65 w/o Cu. The specimens were placed in large cylindrical Al_2O_3 crucibles (6 mm dia. × 42 mm tall), which could accommodate large sample sizes in order to provide sufficiently strong diffraction signals.

TABLE I. POWDER DATA

Powder	Purity	Mesh Size	Average Particle Radius	Shape	Supplier
Copper	99.9 w/o <1,000 ppm O_2	-170 + 400	23.09 µm**	Spherical*	Alfa Aesar
Nickel	99.90 w/o	-48 + 150	80.50 µm*	Spherical*	Alfa Aesar

Verified via optical microscopy*, SEM* and a Horiba CAPA–700 particle size analyzer**

Neutron diffraction experiments were conducted in the C2 powder diffractometer located at the National Research Universal (NRU) research reactor at the Chalk River Laboratory, Chalk River, Canada.[11,12] The crucibles were placed into cylindrical vanadium containment canisters, which were centered/aligned in the body of the vacuum furnace and the diffractometer. A planar silicon single crystal monochromator was used via the 531 reflection and 92.7° takeoff angle to generate a monochromatic incident beam having a wavelength of 0.133069 (7) nm. Calibration and alignment of the instrument were performed prior to experimentation via Rietveld analysis using the General Structure Analysis System (GSAS) code on an external powder standard at room temperature (Si 640c; National Insitute of Standards & Technology (NIST)).

Diffraction patterns spanning 20°–100° in 2θ (with a 0.1° step size) were collected during 1 min time sequences/steps (or data sets) during the sintering cycles. These data sets could be summed over sequential 5 min periods to improve signal quality at the expense of time resolution. Multiple experiments were conducted at different heating rates (10°C–40°C/min), processing temperatures T_P (1,080°C–1,200°C) and isothermal hold durations in a 99.998 v/o dynamic nitrogen atmosphere (Table II).

Sample no. 1 consisted of a preliminary experiment performed on a pure copper powder sample. Sample no. 2 consisted of a preliminary experiment in which an alumina powder barrier layer was used to divide two separate copper and nickel powder layers within the crucible, thus preventing any copper–nickel interactions. Slow heating rates were used to allow complete temperature equilibration of the sample and to initially characterize the evolving, interaction-free nickel and copper peaks within the ND patterns using GSAS.

Sample temperatures were measured using redundant thermocouples. These measurements were verified by tracking the Al_2O_3 peak positions, which inevitably contributed to the diffraction signal, but without overlap or interaction issues with

the (200) face-centered cubic (FCC) copper/nickel peaks. The resulting shifts of the Al_2O_3 reflections due to thermal expansion of the inert alumina crucible thus served as a an internal temperature reference.[13] It should be noted that the temperature variation from the top to the bottom of the crucible was 50°C.[14] The temperature quoted throughout this paper is that determined from the ND signal collected from the entire Al_2O_3 crucible and therefore represents the average temperature of the specimen. Following the ND experiments, samples were prepared using standard metallographic techniques.

RESULTS AND DISCUSSION

Following a presentation of preliminary experiments on the pure copper and non-interacting copper–nickel samples, the ND results will be presented according to the metallurgical stages of TLPS, namely, (1) solid-state sintering during heat-up, (2) melting/dissolution, (3) diffusional or isothermal solidification, and (4) homogenization. A description of the important TLPS stages in liquid-rich systems is described elsewhere.[1,4,15]

Preliminary Experiments

Figure 1 illustrates a series of ND patterns, or data sets, acquired/summed over 5 min time intervals for pure copper powder heated to 1,112°C and then cooled. After a series of patterns was collected at room temperature, all the peaks shifted to lower diffraction angles due to the thermal expansion of the copper and Al_2O_3 as temperature increased. Once a temperature above 1,085°C is reached, the complete disappearance of the copper (200) diffraction peak (and the entire copper diffraction pattern not shown in Figure 1) confirms that the copper phase has undergone melting. As such, the in situ ND technique is effective in detecting the copper melting event.

Figure 2 illustrates ND patterns for the noninteracting copper–nickel specimen (no. 2) at selected temperatures below and above the melting point of pure copper. As in Figure 1, both the copper (200) and nickel (200) diffraction peaks shift to lower angles due to thermal expansion until the copper (200) peak disappears above the melting point of copper. Upon cooling from the high-temperature segments, the liquid copper appeared to have solidified directionally. This is evidenced by the reappearance of larger copper (220) peaks, generating a significant degree of solidification texture only in this experiment employing the Al_2O_3 powder barrier. The nickel (200) peak is clearly stable over the entire temperature range up to 1,178°C. In addi-

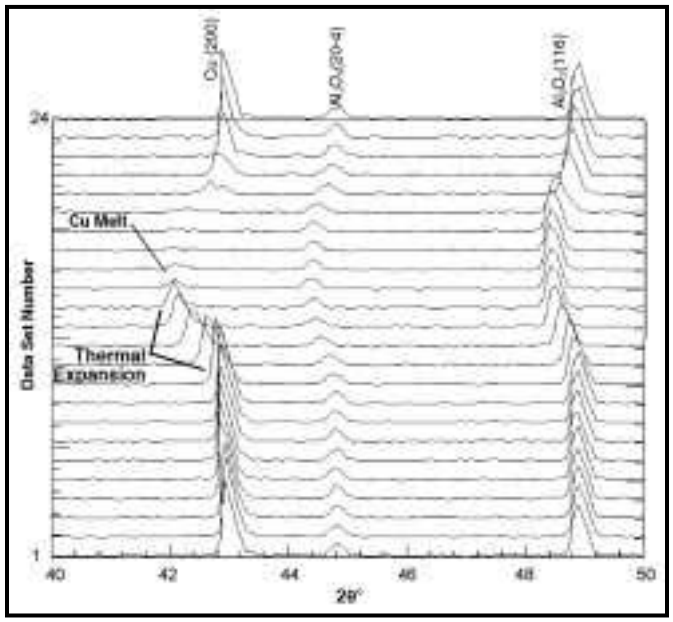

Figure 1. *Three-dimensional plot of diffraction pattern evolution at 5 min intervals for pure copper powder heated to 1,112°C and then cooled (sample 1)*

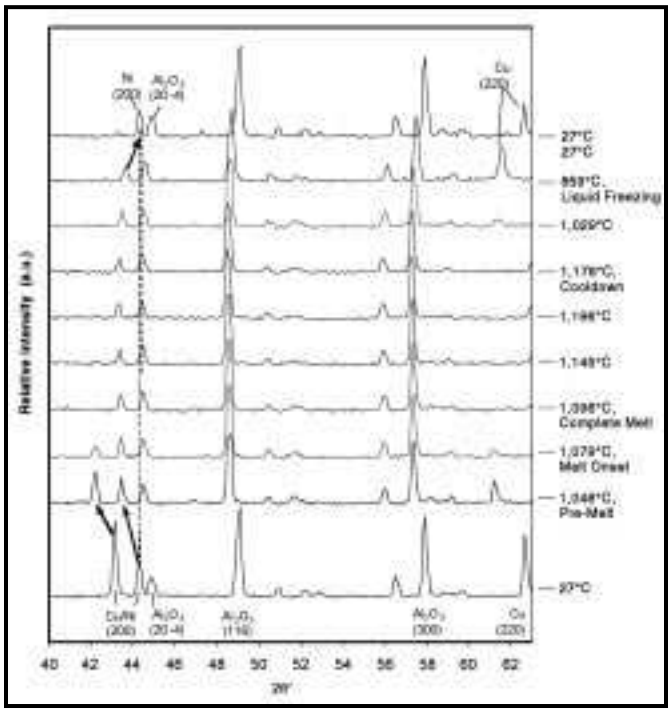

Figure 2. *5 min ND patterns collected in situ for a Ni-65 w/o Cu non-interacting mixture (sample 2). The nickel and copper powders were separated by an alumina barrier. The mixture was slowly heated to 1,096°C, isothermally held at 1,145°C, and 1,196°C, and cooled to 27°C*

tion, upon cooling back to room temperature, the nickel (200) peak returns to its original 2θ position, as indicated by the dashed vertical line. This confirms that the alumina barrier was effective in preventing interdiffusion between the copper and nickel and that the heating and cooling of the nickel powder does not alter its 2θ diffraction line positions, other than reversible shifting due to thermal expansion. As will be shown subsequently, interaction between the nickel and copper powders during TLPS creates an evolving copper/nickel (200) diffraction profile that is significantly different from the behavior exhibited in Figure 2.

Solid-State Sintering and Interdiffusion Prior to Melting

Before an analysis of ND patterns from interacting powders is presented, it is important to note that the lattice parameter of copper–nickel solid solutions at a given temperature (a_{alloy}) varies linearly from a_{Cu} to a_{Ni} (the elemental lattice parameters);[16] it is given by:

$$a_{alloy} = a_{Cu}C_{alloy} + a_{Ni}(1-C_{alloy}) \quad (1)$$

where C_{alloy} is the fractional copper concentration in the alloy. For cubic systems such as FCC nickel and copper, the peak positions q of a given hkl reflection are given by:

$$a^2 = \frac{\lambda^2}{4\sin^2\theta}(h^2 + k^2 + l^2) \quad (2)$$

Substitution of equation (2) in (1) yields:

$$\sin\theta_{alloy} = \left(\frac{C_{alloy}}{\sin\theta_{Cu}} + \frac{1-C_{alloy}}{\sin\theta_{Ni}}\right)^{-1} \quad (3)$$

In equation (3), θ_{Cu} and θ_{Ni} are the diffraction angles of the pure copper and pure nickel *hkl* reflections respectively. θ_{alloy} is the diffraction angle of the same *hkl* reflection corresponding to a given homogeneous alloy composition. Consequently, the 2θ axis in diffraction patterns for isomorphous copper–nickel alloys is analogous to composition (i.e., decreasing copper concentration from the copper peak position to the nickel peak position).[9] Equation (3) can be used to estimate the expected (200) reflection position for a 65 w/o copper specimen (i.e., C_O).

Figure 3(a) shows an isolated nickel–copper contact from a 65 w/o copper mixture after solid-state sintering during heat up to 1,075°C and immediate cooling. The energy dispersive spectroscopy (EDS) line scans for copper and nickel clearly indicate that interdiffusion between pure copper and nickel particles has occurred in the neck regions. This typical interdiffusion profile illustrates the isomorphous nature of the copper–nickel binary system, where solid solutions of any intermediate composition can form.

Figure 4 is a "film plot" showing the evolution of diffraction patterns over time during prolonged solid-state sintering of a 65 w/o copper powder mixture (sample 3). This graphical presentation technique[17] provides a useful means of tracking the evolution of peaks (i.e., dark lines) over numerous sequential 1 min diffraction patterns (i.e., "data sets") along the ordinate axis. This specimen was heated to 1,080°C at 40°C/min, (just below the copper melting point), held for 630 min, and cooled. The initial diffraction patterns

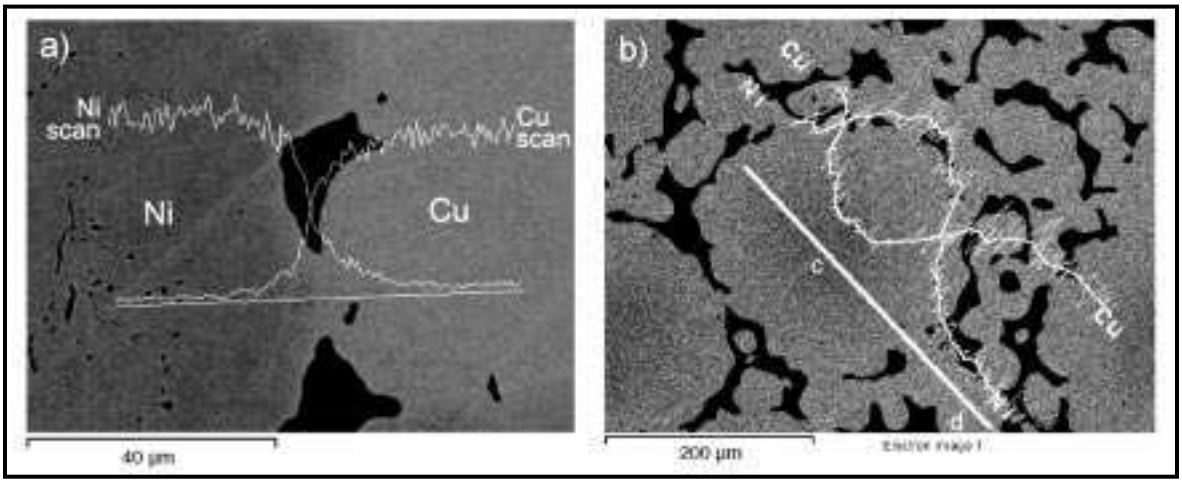

Figure 3. *Backscattered electron images (BSE) and EDS line scans showing copper–nickel interdiffusion profiles between contacting solid-state-sintered particles: (a) during heat-up to 1,075°C, and (b) after 630 min at 1,080°C*

collected at room temperature show stable copper and nickel (200) peaks at 42.24° and 44.42°, respectively, as well as Al_2O_3 peaks ((20-4) at 44.99° and (116) at 49.11°).

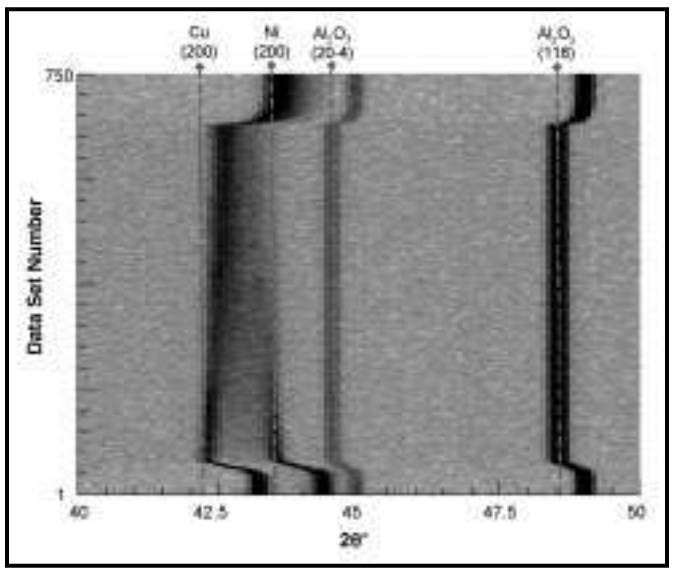

Figure 4. *Film plot of in situ diffraction pattern evolution collected at 1 min intervals during solid-state sintering of a Ni-65 w/o Cu powder mixture heated to 1,080°C for 630 min (sample 3)*

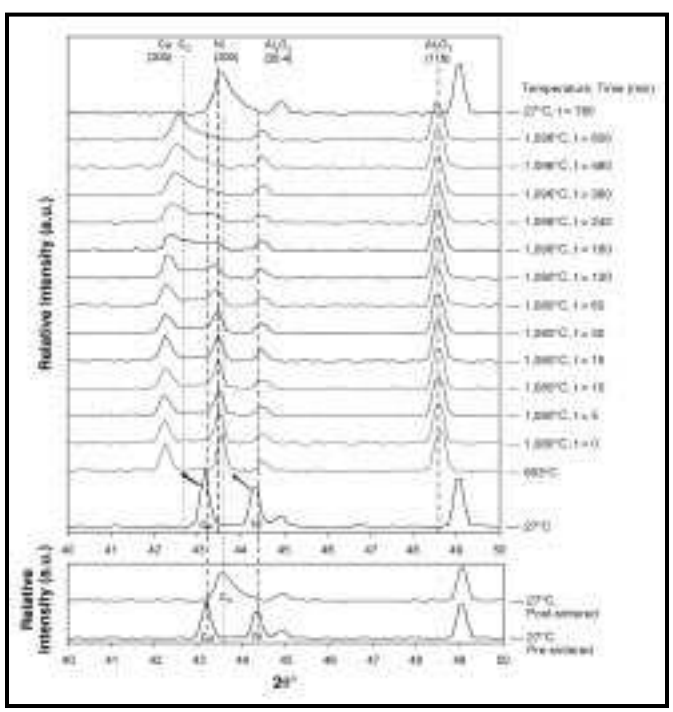

Figure 5. *5 min ND patterns collected in situ during the isothermal segment of a solid-state-sintered Ni-65 w/o Cu powder mixture at 1,080°C (sample 3). Bottom plot directly compares presintered and postsintered diffraction patterns at room temperature*

During heat-up, all peaks shift to lower angles due to thermal expansion of the respective lattices. Vertical dashed lines have been included to mark the positions of key high-temperature peaks. Once the isothermal processing temperature is reached (T_P = 1,080°C), the alumina peaks cease to shift. However, as the sample is held at this temperature, ongoing copper–nickel interdiffusion causes noticeable asymmetric broadening effects in both the copper and nickel peaks. The developing alloy regions within the sample cause inward broadening of the initial elemental copper and nickel diffraction peaks, as well as increasing diffraction intensities at intermediate angles between them over time. Upon cooling after the isothermal hold, a broad diffraction profile still exists at room temperature. However, it is clear that the most intense portion of this profile has a diffraction angle between that of the original pure copper and pure nickel peaks. As the micrograph in Figure 3(b) indicates, this broad peak is attributed to the significant compositional gradients that still remain between the nickel particle core (point c) and the sintered copper particles (point d) at the end of this experiment.

Figure 5 shows time–temperature resolved patterns acquired over 5 min sequences (summations of five 1 min data sets) at discrete points during the sintering cycle to more clearly show the evolution of two dimensional patterns. The pre-sintered and post-sintered patterns (bottom) show that solid-state interdiffusion for over 600 min has generated a broad alloy peak indicative of a partially homogenized sample, Figure 1. The centroid of the alloy peak is in agreement with that expected for the copper-rich bulk composition of the sample (dashed line at C_O = 65 w/o copper). While the centroid of the post-sintered peak corresponds closely to the lattice parameter for a 65 w/o copper mixture, it is clear that a significant "tail" in the peak exists toward higher 2θ angles, indicating that some nickel-rich regions are still present in the sample after 600 min at temperature.

Close examination of Figure 5 reveals that even after 120 min at 1,080°C, there exists near-pure copper and nickel regions in the sample. Note that the furnace temperature rose slightly after this 2 h hold but enough interdiffusion occurred prior to this point such that liquid should not have formed up to 1,096°C (i.e., the sample still constitutes a solid-state-sintered case). At this

slightly higher temperature, and for times ranging from 180 to 600 min, the maximum peak intensity begins to shift away from the pure-copper position and the distinct peak at the pure nickel 2θ position disappears. This is consistent with the EDS line scan of Figure 3(b) which shows a measurable copper concentration at the core of the nickel particle.

Figure 6 shows diffraction patterns collected immediately prior to melting for specimens heated below 1,085°C at different heating rates (10°C and 40°C/min). In comparison, a diffraction pattern for sample 2 is included, which contained an alumina powder barrier preventing any copper and nickel interdiffusion from taking place. Sample 5, which was slowly heated at 10°C/min, appears to have higher diffraction intensities at intermediate angles between the pure copper and pure nickel peak positions, which would indicate a higher degree of interdiffusion and alloying. However, the difference between the 10°C and 40°C/min data is minor. This can be attributed to the limited sensitivity of this technique, and to the low degree of interdiffusion that has occurred during these short heating regimes.

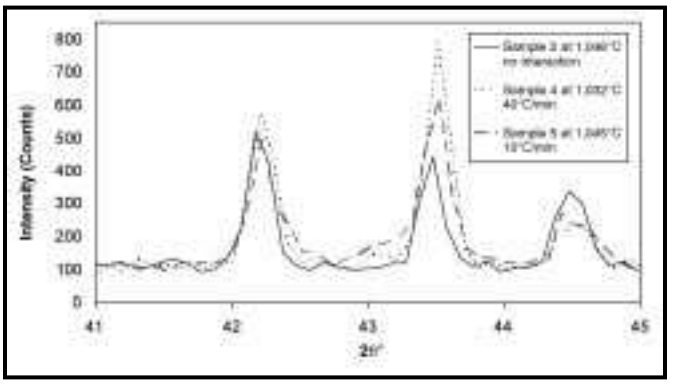

Figure 6. *Comparison of peak profiles for diffraction patterns collected immediately prior to melting in samples heated at different heating rates*

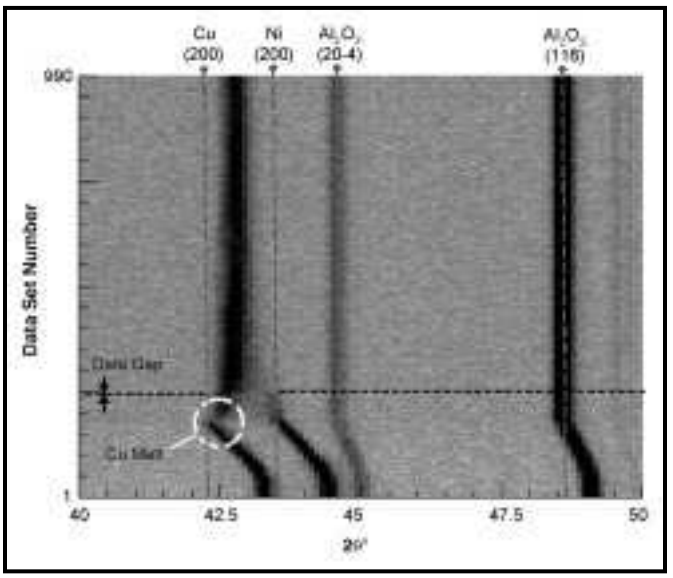

Figure 7. *Film plot of in situ diffraction pattern evolution collected at 1 min intervals during TLP sintering of a Ni-65 w/o Cu powder mixture heated to 1,128°C for 900 min (sample 5)*

Melting and Dissolution

Figure 7 shows the evolution of diffraction patterns during TLP sintering of sample 5. This specimen was heated to 1,128°C at 40°C/min to form a copper-rich liquid phase, held for 900 min, and cooled. This plot illustrates different sintering and interdiffusion behavior in contrast to the solid-state-sintered specimen, Figure 4. In this case, a clear melting event is observed by the removal of copper peaks, evidenced by a break in the copper (200) curve at 1,085°C (circled). The nickel peaks persist since a portion of the mixture remains solid/crystalline at the sintering temperature (i.e., the nickel particles). Immediately after melting, a slightly shifted (higher 2θ) copper-rich diffraction peak appears to grow in intensity as the pure-nickel intensity decreases over time. Concurrently, diffraction intensities gradually increase at intermediate 2θ angles due to interdiffusion, or solute uptake, by the solid-nickel particles.

Due to reactor flux variations, 63 min of data could not be collected during the isothermal segment as well as the cool-down segment. Nonetheless, the interdiffusion process (i.e., solute uptake by solid-nickel particles) appears to be much more rapid during liquid-phase sintering vs. the solid-state sintering. This is clear when comparing the film plots of specimens 2 and 5 (Figures 4 and 7). The presence of the liquid phase during sintering at 1,128°C generates a much more uniform distribution of solute over the wetted nickel particles, which will accelerate the solute-uptake process.

In order to further analyze ND pattern evolution during TLPS, it is necessary to examine time–temperature resolved data for sample 5, Figure 8. At 1,075°C, distinct copper and nickel peaks are present during what is referred to as the "premelt" condition during heat-up. At the average sample temperature of 1,078°C, the onset of copper melting is first detected and this is designated as the start of the liquid-phase regime (post-melt time = 0

min). At this point, copper regions at the top of the crucible (the hottest furnace region) have begun to melt and this causes an abrupt decrease in the pure-copper peak intensity. It should be noted that the copper peak in the pattern at t = 0 exhibits a clear shoulder at intermediate angles. This diffraction signal originates from sintered neck alloy regions of the specimen having copper-rich compositions less than or equal to the phase diagram solidus composition. Therefore, they will not melt at 1,085°C since they constitute stable solid solutions. In the 1,095°C, t = 5 min pattern, only this shifted residual shoulder peak remains, which will be referred to as the solidus peak (or C_S).

Isothermal Solidification

After the melting event in Figure 8, the copper-rich C_S (200) peak appears to grow rapidly in intensity while the pure-nickel peak intensity decreases slowly (time segments 5 min through 60 min). This indicates that a copper-rich solid solution is rapidly forming within the two-phase liquid–solid specimen during the isothermal segment. This supports nonisothermal DSC and metallographic results, where rapid liquid removal rates at short times via isothermal solidification would leave behind a copper-rich layer (composition near C_S) that surrounds the still solute-deficient nickel particles.[4] As the heavy dashed line in Figure 8 indicates, the 2θ peak location for the maximum intensity of the copper-rich peak remains fixed at the CS location up to the 60 min diffraction pattern. This is due to the continued presence of liquid phase which dictates, through interface equilibrium considerations, that the solid adjacent to the liquid–solid interface remain at C_S. Once all the liquid has isothermally solidified, this restriction on the interfacial solid composition is removed. Beginning with the 145 min diffraction pattern, the 2θ peak location for the maximum intensity of the copper peak begins to shift to higher 2θ until it reaches a position that corresponds to the bulk composition of the mixture, C_O. This indicates that complete isothermal solidification occurred near 145 min, which is consistent with a previous analysis using DSC.[4] Over the same time frame, solute diffusion deeper into the nickel particles eventually causes the nickel peaks to be completely removed after 145 min. After 900 min at 1,128°C, a sharp single peak is formed, indicating that a homogeneous composition has been established, which is in good agreement with the bulk mixture composition (C_O = 65 w/o copper).

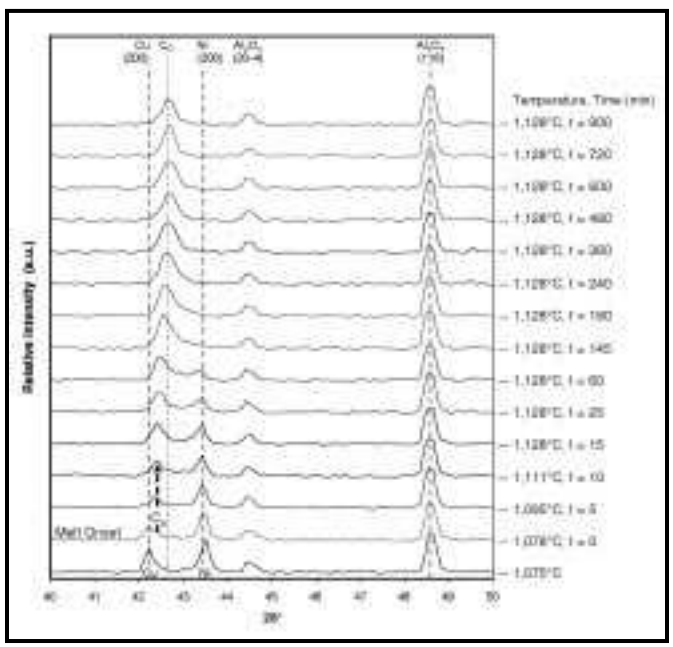

Figure 8. ND patterns collected at 5 min intervals during the isothermal solidification stage of a Ni-65 w/o Cu powder mixture sintered at 1,128°C (sample 5)

As Table II indicates, multiple TLPS experiments were conducted at different isothermal processing temperatures to investigate the effects on liquid formation, dissolution, and the general ND profile

TABLE II. NEUTRON DIFFRACTION EXPERIMENTS

Sample No.	Powder Mass (g)	C_O (w/o Cu)	Atmosphere	R_h (°C/min)	T_P (°C)	Hold Time at T_P (min)	Experiment
1	2.522	100.0	N2	40	1,112	30	Pure-copper melt characterization
2	2.140	64.0	N2	N/A	1,096–1,196	60	Non-interacting, slow heating
3	2.515	65.2	N2	40	1,080	630	Solid-state sintering
4	2.523	65.0	N2	40	1,091	1,040	TLPS
5	2.529	65.3	N2	10	1,128	900	TLPS
6	2.495	65.0	N3	40	1,162	10	TLPS
7	2.502	65.0	N2	40	1,178	720	TLPS
8	2.490	64.8	N2	40	1,194	30	TLPS

evolution behavior. Figure 9 shows diffraction patterns collected immediately after the onset of melting (5 min) for six samples heated to different peak temperatures. A diffraction pattern for specimen 3 is also shown, which was solid-state sintered at 1,080°C and is included for relative comparisons with the other LPS specimens. Note: the diffraction patterns for the 1,194°C and 1,178°C specimens contain molybdenum (200) peaks originating from the molybdenum sample canisters used for these particular higher-temperature experiments. Vertical dashed lines have been included to identify the pure-nickel and -copper peak positions at 1,085°C, where copper melting occurs and the pure-copper lattice becomes unstable. These lines are useful in interpreting small peak shifts during sintering at different temperatures.

In Figure 9, the nickel and Al_2O_3 peaks shift to lower angles at higher temperatures due to thermal expansion. Conversely, the residual copper-rich C_S peaks (post-melt) show a distinctively different trend since they are shifted to higher 2θ angles. This is due to superimposed compositional shifting effects and the fact the pure copper is no longer stable at these temperatures. As the sintering temperature increases, the copper–nickel phase-diagram solidus indicates that the solubility of copper in nickel (C_S) decreases with increasing temperature (becoming more nickel rich). For the diffraction pattern at 1,091°C, the unmelted, residual interdiffusion regions can have very high copper contents close to pure copper. Accordingly, Figure 9 shows that the post-melt C_S peak at 1,091°C is shifted minimally relative to the pure copper peak at 1,080°C. Higher temperatures show increased compositional shifting due to decreasing C_S (or increasing nickel solubility). However, after only 5 min there are only minor differences in the patterns for each sample and a considerable fraction of the nickel-particle core remains unalloyed.

Figure 10 shows diffraction patterns collected 15 min after melting and temperature stabilization. At this point the residual C_S peaks have already grown significantly. At higher temperatures, the C_S peaks are smaller (due to increased melt-back of solid-state alloyed regions) and the nickel peaks are also smaller due to nickel dissolution. This is most clear when comparing the total diffraction profile areas with the fully solid 1,080°C case (areas above the horizontal dashed lines). This is indicative of the decreasing total volume fraction of solid-solution material within the liquid–solid mixtures due to dissolution (increased liquid formation) at higher T_P. It is also clear that there is a reduction of the intermediate alloy range Δθ between the copper-rich and nickel peaks since C_S is becoming increasingly nickel-rich (shifted to higher 2θ angles) and smaller compositional gradients are possible within the solid particles.

The isothermal solidification mechanism in TLPS can be more clearly elucidated by plotting the 2θ position of the rapidly growing copper-rich solid-solution peaks at the various processing temperatures. Figure 11 shows the nickel and (C_S) peak positions measured at half maximum for all specimens shortly after the melting event. The shifting peak positions of each sample are plotted according to their respective peak processing temperature (T_P) on the ordinate axis. It should be noted that at short times (0 to 10 min) many of the samples were still equilibrating to their peak

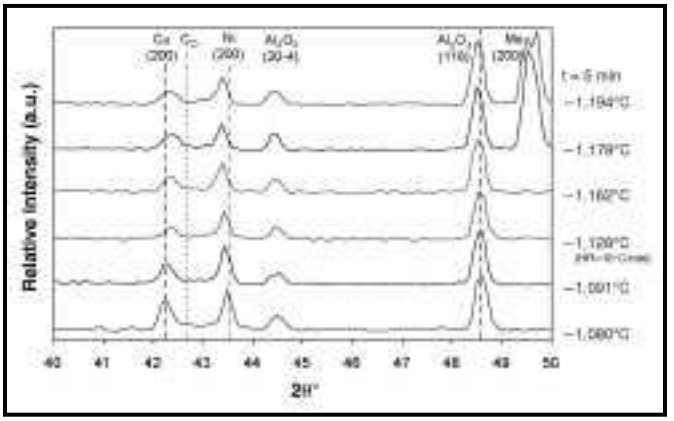

Figure 9. *ND patterns collected 5 min after the melting event for Ni-65 w/o Cu powder mixtures isothermally held at different process temperatures*

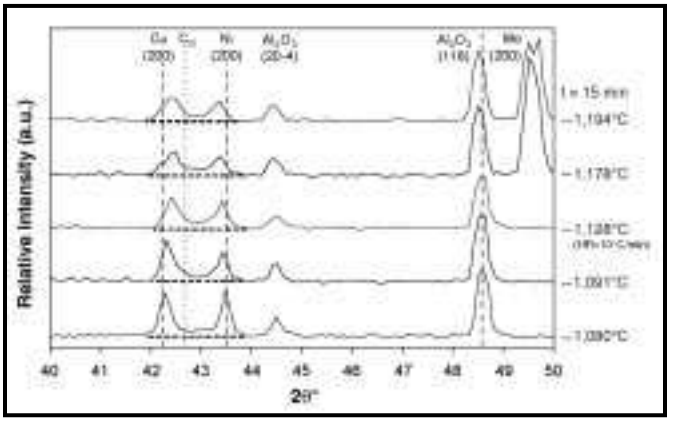

Figure 10. *ND patterns collected 15 min after the melting event for Ni-65 w/o Cu powder mixtures isothermally held at different process temperatures*

isothermal processing temperature. The presentation format in Figure 11 is somewhat similar to a film plot, but these data summarize the melting behavior of all specimens as they are heated to their respective T_P from 1,080°C to 1,194°C. The peak positions at t = 5 min and 10 min have been connected for the different specimens to trace the peak positions at similar times when sintering at different T_P. The nickel peaks after 5 min and 10 min shift to lower 2θ angles due to thermal expansion at higher temperature. The degree of expansion is in agreement with calculations based on the known temperature-dependent expansion of the nickel lattice (dark dashed line in Figure 11).[18]

The copper-rich peaks at 5 min and 10 min are also plotted shortly after the melting event. At these times, the copper peaks show a distinctly different behavior relative to the nickel peaks. Rather than shifting to lower angles due to thermal expansion, the residual peaks shift to higher angles at increasing T_P due to compositional effects. A theoretical curve for the expected expansion of pure copper (if it were stable) is also included. This theoretical curve is calculated by extrapolating copper-expansion data[18] and illustrates the divergent behavior of the copper peaks upon melting (thermal shifting vs. compositional shifting effects). As the typical film plot in Figure 7 shows, as well as Figure 9, all specimens exhibited this characteristic copper melting behavior above 1,085°C, namely, melting of unstable pure copper regions leaving behind copper-rich solid-solution regions responsible for the C_S peaks, which grow rapidly immediately after melting.

Based on the known temperature-dependent thermal-expansion coefficients of the copper and nickel lattices,[18] equation 3 can be used to estimate the composition of the solid-solution alloy regions responsible for generating the C_S peaks. These data are plotted vs. sintering temperature and superimposed on the copper–nickel phase diagram in Figure 12.[19] The in situ results show good agreement with the solidus line of the phase diagram. Discrepancies are likely due to temperature gradients within the samples as they equilibrate to their respective T_P. However, this datum affirms, in situ, that the isothermal solidification mechanism responsible for liquid removal during copper–nickel TLPS occurs via the epitaxial growth of a copper-rich solid solution (at C_S) surrounding the solid base-metal particles, and limited long-range diffusion into the nickel core.

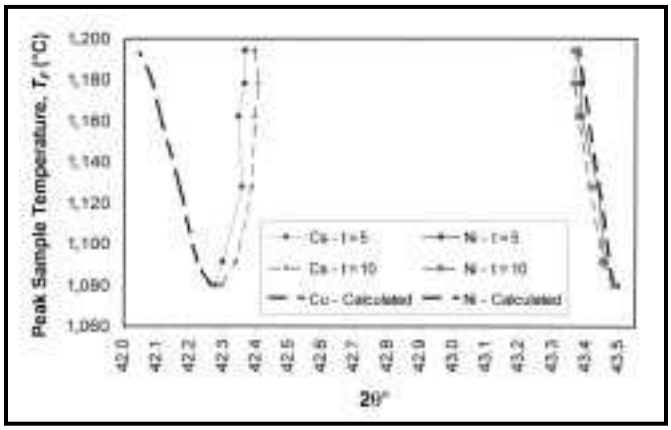

Figure 11. *Cu, Ni, and C_S peak positions at t = 5 min (after melt onset) and 10 min for samples 3–8 (i.e., 1,080°C–1,094°C)*

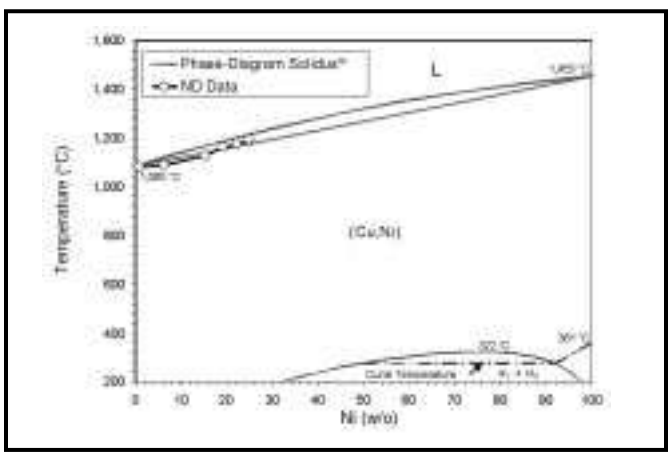

Figure 12. *Calculated C_S diffraction peak compositions in comparison with the copper–nickel phase-diagram solidus line[19]*

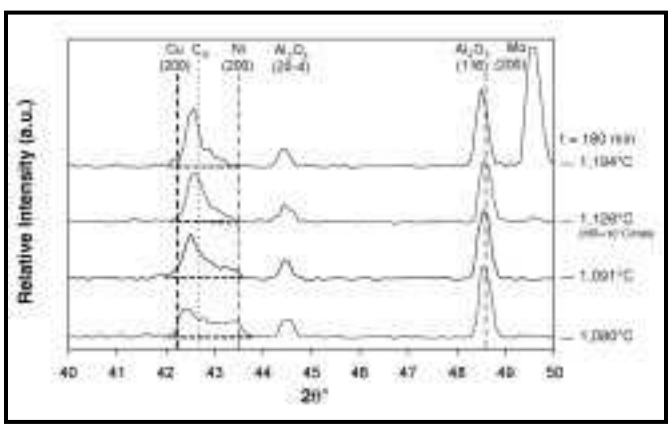

Figure 13. *ND patterns collected 180 min after the melting event in Ni-65 w/o Cu powder mixtures isothermally held at different process temperatures*

Homogenization

Figure 13 shows diffraction patterns for samples that were held at different T_P for a much

longer duration (180 min), where DSC results[4] indicate that the liquid phase should be fully solidified. The solid-state-sintered specimen at 1,080°C still exhibits a bimodal ND profile, indicating a much less homogenous composition. In comparison, the profiles of the specimens TLP sintered above 1,085°C clearly show that the presence of a liquid phase has accelerated the evolution of a more refined single peak and therefore a more homogeneous specimen composition. The liquid phase effectively increases the net rate of interdiffusion and solute uptake into and surrounding the nickel solid-solution particles.

However, Figure 13 indicates that, even after 180 min, the TLPS samples are not completely homogeneous since the peaks at each hold temperature are still somewhat broad and asymmetric. Also, the peak maxima positions are to the left (lower 2θ angles) of the expected positions for homogeneous alloys at C_O. Compositional inhomogeneity is also evidenced by the nickel-rich "tail" at the right of each diffraction profile, which decreases with increasing T_P. This is consistent with DSC results[4] where samples held at 1,140°C for similar times (i.e., 150 min) still exhibited a broad melting event and therefore a broad compositional range. Diffraction patterns collected at longer times (as in Figure 8) show that complete homogenization occurs with further sintering at each T_P.

CONCLUSIONS

This study has shown that ND is capable of identifying the melting event during sintering of copper and nickel powder mixtures as well as the ongoing interdiffusion process taking place during TLPS at elevated temperatures. By monitoring the evolution of copper–nickel solid-solution diffraction peak profiles in situ, this technique has shown that isothermal solidification of the liquid phase occurs primarily by the epitaxial growth of a copper-rich "layer" surrounding the nickel-rich base-metal particles. This is evidenced by the rapid growth of residual "C_S" diffraction peaks immediately after the melting event, whose 2θ position is coincident with that predicted by the phase-diagram solidus. With increasing sintering times, homogenization of the powder mixtures eventually causes a sharp, single-peak profile to be generated. This characteristic profile evolution is significantly accelerated when a liquid phase is formed (i.e., TLPS vs. solid-state sintering).

ACKNOWLEDGMENTS

This work was supported by the Canadian Neutron Beam Centre (CNBC) and the National Sciences and Engineering Research Council of Canada (NSERC). The authors would also like to thank Erik Szakaly for contributions regarding metallographic work.

REFERENCES

1. R.M. German, *Sintering Theory and Practice,* 1996, Wiley-Interscience Publications, New York, NY.
2. S.F. Corbin and D.J. McIsaac, "Differential Scanning Calorimetry of the Stages of Transient Liquid Phase Sintering", *Mater. Sci. Eng. A,* 2003, vol. A346, no. 1–2, pp. 132–140.
3. S.F. Corbin and P. Lucier, "Thermal Analysis of Isothermal Solidification Kinetics During Transient Liquid-Phase Sintering", *Metall. Mater. Trans. A,* 2001, vol. 32A, no. 4, pp. 971–976.
4. D.M Turriff and S.F. Corbin, "Quantitative Thermal Analysis of Transient Liquid-Phase-Sintered Cu-Ni Powders", *Metall. Mater. Trans. A,* 2008, vol. 39, no. 1, pp. 28–38.
5. F.J. Puckert, W.A. Kaysser and G. Petzow, "Transient Liquid Phase Sintering of Ni-Cu", *Z. Metallkde,* 1983, vol. 74, no. 11, pp. 737–743.
6. R.M. German and J.W. Dunlap, "Processing of Iron-Titanium Powder Mixtures by Transient Liquid Phase Sintering", *Metall. Trans. A,* 1986, vol. 17A, no. 2, pp. 205–213.
7. W.H. Baek and R.M. German, "Transient Liquid Phase Sintering in the Fe-Fe_2Ti System", *Int. J. Powder Metall.,* 1986, vol. 22, no. 4, pp. 235–244.
8. R.N. Lumley and G.B. Schaffer, "The Effect of Solubility and Particle Size on Liquid Phase Sintering", *Scripta Mater.,* 1996, vol. 35, no. 5, pp. 589–595.
9. B. Fisher and P.S. Rudman, "X-ray Diffraction Study of Interdiffusion of Cu-Ni Powder Compacts", *J. Applied Physics,* 1961, vol. 32, no. 8, pp. 1,604–1,612.
10. R. Delhez, E.J. Mittemeijer and E.A. van den Bergen, " X-ray Diffraction Line Profile Analysis of Diffusional Homogenization in Powder Blends", *J. Mater. Sci.,* 1978, vol. 13, no. 8, pp. 1,671–1,679.
11. M. Potter, H. Fritzsche, D.H. Ryan and L.M.D. Cranswick, "Low-Background Single-Crystal Silicon Sample Holders for Neutron Powder Diffraction", *J. of Appl. Crystallogr.,* 2007, vol. 40, no. 3, pp. 489–495.
12. L.M.D. Cranswick, R. Donaberger, I.P. Swainson and Z. Tun, "Convenient Off-Line Error Quantification and Characterization of Concentricity of Two Circles of Rotation for Diffractometer Alignment", *J. of Appl. Crystallogr.,* 2008, vol. 41, no. 2, pp. 373–376.
13. I. Bull, P. Lightfoot, L.A. Villaescusa, L.M. Bull, R.K.B. Gover, J.S.O. Evans and R.E. Morris, "An X-ray Diffraction and MAS NMR Study of the Thermal Expansion Properties of Calcined Siliceous Ferrierite", *J. Am. Chem. Soc.,* 2003, vol. 125, pp. 4,342–4,349.
14. D.M. Turriff, "Process Kinetics of Transient Liquid Phase Sintering in a Binary-Isomorphous Alloy System", 2007, PhD Thesis, University of Waterloo, Waterloo, ON, Canada.
15. D.M. Turriff and S.F. Corbin, "Modelling the Influences of

Solid-State Interdiffusion and Dissolution on Transient Liquid Phase Sintering Kinetics in a Binary Isomorphous System", *Metall. Mater. Trans. A,* 2006, vol. 37A, no. 5, pp. 1,645–1,655.

16. C.S. Barrett, *Structure of Metals, Second Edition,* 1952, McGraw-Hill, New York, NY.
17. B. Hinrichsen, R.E. Dinnebier and M. Jansen, "Powder3D: An Easy to Use Program for Data Reduction and Graphical Presentation of Large Numbers of Powder Diffraction Patterns", *Z. Kristallogr. Suppl.,* 2006, vol. 23, pp. 231–236,
18. Y.S. Touloukian, R.K. Kirby and P.E. Taylor, *Thermophysical Properties of Matter—TPRC Data Series, Vol. 12, Thermal Expansion Metallic Elements and Alloys,* 1979, IFI/Plenum Press, New York, NY.
19. T.B. Massalski, editor, "Ni-Cu Binary Alloy Phase Diagram", *Binary Alloy Phase Diagrams,* 1986, vol. 1, American Society for Metals, Metals Park, OH. ijpm